Size-Specific Infrared Spectra of Benzene-$(H_2O)_n$ Clusters ($n = 1$ through 7): Evidence for Noncyclic $(H_2O)_n$ Structures

R. Nathaniel Pribble and Timothy S. Zwier*

Resonant ion-dip infrared spectroscopy has been used to record size-specific infrared spectra of C_6H_6-$(H_2O)_n$ clusters with $n = 1$ through 7 in the O–H stretch region. The O–H stretch spectra show a dramatic dependence on cluster size. For the $n = 3$ to 5 clusters, the transitions can be divided into three types—attributable to free, π hydrogen-bonded, and single donor water-water O–H stretches—consistent with a C_6H_6-$(H_2O)_n$ structure in which benzene is on the surface of a cyclic $(H_2O)_n$ cluster. In $n = 6$ and 7 clusters, the spectra show distinct new transitions in the 3500 to 3600 wave number region. After comparison of these results with the predictions of ab initio calculations on $(H_2O)_n$ clusters, these new transitions have been assigned to double donor O–H stretches associated with the formation of a more compact, noncyclic structure beginning with $(H_2O)_6$. This is the same size cluster for which ab initio calculations predict that a changeover to noncyclic $(H_2O)_n$ structures will occur.

One of the most powerful probes of intermolecular hydrogen bonding (Y···HX) has been the perturbations imposed by the hydrogen bond on the HX stretch vibrational mode. In fact, it has been argued that the HX stretching mode provides one of the clearest and most sensitive means of establishing the presence of hydrogen bonding in a system (*1*).

The H–X stretch distinguishes and characterizes a hydrogen bond by the large red shift in its absorption frequency, the significant increase in its absorption intensity (often by a factor of 10 or more), and the unusual breadth of the transitions (*1, 2*). The H–X stretch is especially sensitive to the number, strength, and type of hydrogen bonds in which it participates because it vibrates directly against the hydrogen bond. Water and the alcohols, for example, whether as liquid or as solid, have strong, broad O–H absorptions that extend from about 3700 to 3100 cm^{-1}, with inhomogeneous broadening dominating the observed breadths (*3*).

Gas-phase clusters provide an important testing ground for theories aimed at understanding the hydrogen bond and its consequences. In particular, the importance and complexity of water has fueled much experimental (*4–13*) and theoretical work (*14–26*) on its gas-phase clusters. Recent progress has been made in characterizing the structures and intermolecular binding in the water dimer and trimer (*4–8*), but difficulties in observing or assigning transitions to a given $(H_2O)_n$ cluster have so far hindered studies of larger clusters (*9–11*). In particular, beginning at $(H_2O)_6$, noncyclic structures are calculated to be near in energy to the S_6 symmetry cyclic water hexamer. The theoretical models differ in their predictions for the relative ordering of these structures (*14, 17–21*), and no definitive experimental test of the ordering currently exists.

Given water's importance as solvent, one also seeks better probes of solute-solvent interactions involving water as solvent. In that case, both the disruption of water's structure imposed by the solute molecule and the site-specific attractions and repulsions between the first shell or shells of water molecules and the solute must be considered. Benzene is a prototypical aromatic incorporated into many biologically important molecules. As a result, benzene-water interactions have been the focus of many studies in the matrix (*27*) and in gas-phase clusters (*28–34*).

Our group recently carried out a resonant two-photon ionization time-of-flight mass spectroscopy (R2PI-TOFMS) study of BW_n clusters with $n = 1$ through 8 (where B is benzene and W is water) (*28*). In that work, benzene served as chromophore for the cluster through its vibronically allowed $S_1 \leftarrow S_0$ transition. Figure 1 presents R2PI spectra in the 6^1_0 region of the $S_1 \leftarrow S_0$ transition of benzene with their cluster size assignment indicated. For $n = 1$ through 5, the R2PI studies (*28*) show that the BW_n^+ clusters formed upon photoionization fragment efficiently by loss of a single water molecule to appear in the BW_{n-1}^+ mass channel. In BW_6 and BW_7, fragmentation by loss of a second water molecule becomes energetically allowed.

In the case of C_6H_6-H_2O, both our R2PI studies and high-resolution microwave spectral studies (*29, 30*) have shown that the water molecule is not rigidly held to benzene but can rotate internally about benzene's sixfold axis and can interchange its π hydrogen-bound hydrogens. In the larger clusters, the vibronic level R2PI spectroscopy is consistent with structures for the BW_n clusters composed of W_n clusters to which benzene is surface-attached (*28*). Further insight to the intermolecular binding, especially between the water molecules, was limited by the fact that the electronic spectroscopy views the water molecules only indirectly in terms of the perturbations imposed on benzene's vibronic transitions.

To address this limitation, we present size-selected infrared (IR) spectra of the BW_n clusters with $n = 1$ through 7 in the O–H stretch region (3000 to 4000 cm^{-1}). These spectra bring new insight not only into BW_n clusters but also into the W_n clusters themselves, especially in the larger clusters. These IR spectra are recorded with a technique we call resonant ion-dip IR spectroscopy (RIDIRS), a variant of a method first introduced by Lee and coworkers (*35*). The IR spectra are taken in a dual beam arrangement in which the ultraviolet (UV) laser used for R2PI is passed twice through the ion source region of the TOF mass spectrometer. A particular BW_n cluster (*36*) is singled out for study by monitoring the ion signal at the appropriate mass in the TOF mass spectrum with the R2PI laser tuned to the dominant transition assigned to this cluster (Fig. 1). Cluster ions created by the two passes of the laser are

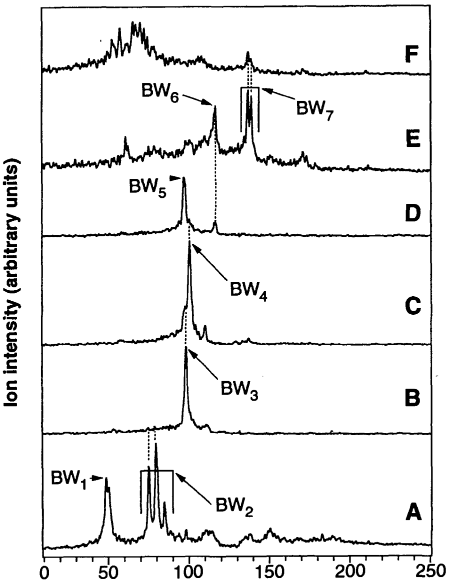

Fig. 1. (**A** to **F**) Resonant two-photon ionization spectra of BW_n with $n = 1$ through 7 monitoring the BW_n^+ mass channels with $n = 1$ through 6. The indicated transitions are those monitored for cluster size selection in the RIDIR spectra. Assignments for the transitions are taken from (*28*).

Department of Chemistry, Purdue University, West Lafayette, IN 47907–1393, USA.

*To whom correspondence should be addressed.

born at different potentials in the ion source and arrive at the microchannel plate ion detector at slightly different times (~100-ns separation). One of the UV beams is overlapped with the optical parametric oscillator (OPO) output (37), which precedes the R2PI laser by 100 to 500 ns. When an IR absorption out of the same ground-state level as that monitored by the R2PI laser is encountered, a decrease in the ion signal from the overlapped beam is observed. With proper normalization of the two ion signals, the fractional depletion in ion signal is monitored as a function of OPO wavelength. The dual beam method removes a major source of noise in the depletion experiment arising from shot-to-shot laser power fluctuations in the R2PI laser.

Overview RIDIR spectra of the BW_1 to BW_7 clusters in the O–H stretch region are shown in Fig. 2. The frequencies and breadths of the transitions are listed in Table 1. Depletions near 100% on the strongest transitions are possible at high OPO power. This saturation affects the relative intensities observed and likely to some extent the breadths of the transitions.

Several points can immediately be made about the spectra. First, for each BW_n cluster (besides $n = 1$), the number of resolved O–H stretch transitions is approximately equal to the number of O–H groups present in the cluster. The spectra thus give a near-complete picture of the O–H stretch vibrations in each BW_n cluster. The fact that virtually all transitions carry significant intensity may result from the reduced symmetry and perturbed force constants of the W_n clusters imposed by benzene's presence. Partial saturation of the transitions also contributes to the observation of even weak transitions. The presence of "extra" transitions in the BW_1 spectrum (Fig. 2A) arises from the presence of *ortho* and *para* H_2O in the expansion. An analysis of this spectrum will be given elsewhere (38).

Second, the development of the spectra with increasing cluster size reflects the sensitivity of the water molecule to its hydrogen bonding environment. For $n = 1$ through 6, the lowest frequency transitions shift about 100 cm^{-1} lower in frequency with the addition of each successive water molecule to the cluster. Because the highest frequency transitions are virtually unchanged with cluster size (~3715 cm^{-1}), the larger BW_n clusters exhibit an enormous spread in O–H stretch frequencies extending down to the C–H stretch transitions near 3100 cm^{-1}. This range spans that observed in liquid water and ice (3). In contrast, the C–H stretch of C_6H_6, present as a triad of sharp, weak transitions near 3100 cm^{-1} (barely visible in these overview scans), remains unchanged in frequency even when as many as seven water molecules are added to the cluster (38).

Third, the breadths of the transitions also show a clear development with cluster size and frequency. For clusters containing no more than three water molecules, all transitions are in the range from 2 to 5 cm^{-1}, reflecting the combined effects of rotational structure and OPO bandwidth. In the larger clusters, transitions with large red shifts are significantly broadened to as much as 30 cm^{-1} full width at half maximum (FWHM) (Table 1).

Finally, the expectation for BW_n is that the intensities of the O–H stretch transitions should also depend sensitivity on BW_n cluster size (*14, 15*). Such sensitivity is reduced by saturation of the transitions in the present experiment. Nevertheless, a qualitative increase in the per-water integrated intensity is observed.

In discussing the spectra of the BW_n clusters, data on the W_n clusters themselves provide useful points of comparison. In Table 2 we list the observed O–H stretch absorptions in BW_n and compare these absorptions, where possible, with gas-phase data (8), matrix data (*12*), and ab initio calculations (*14–16, 39*) on the pure water clusters. The experimentally determined (W_2, W_3) and calculated (W_n, $n > 3$) lowest energy water cluster structures are shown in Fig. 3 in schematic form, highlighting the types of O–H bonds present in the W_n clusters.

The O–H stretch transitions of BW_2 occur at frequencies very close to those of

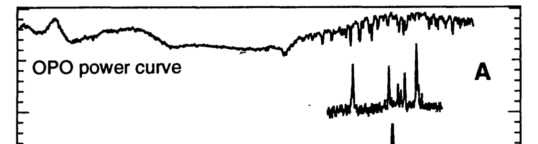

Fig. 2. (**A** to **G**) Overview RIDIR spectra of BW_n with $n = 1$ through 7 in the O–H stretch region. The idler OPO power as a function of wavelength is shown above the spectrum in (A). The spectra are uncorrected for this power change. The dip in power in the region from 3450 to 3500 cm^{-1} is attributable to O–H absorption in the $LiNbO_3$ crystal, whereas the sharp dips in power at high frequency are attributable to water vapor absorption.

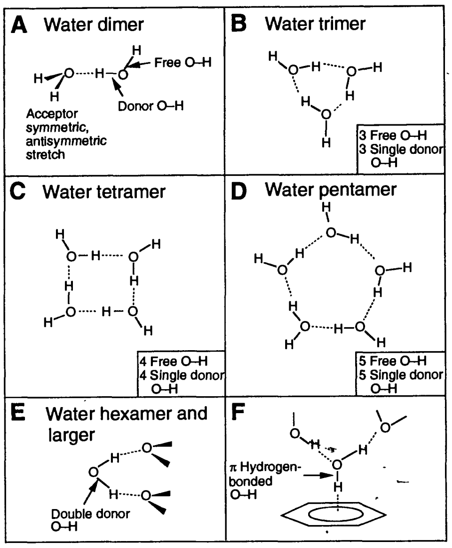

Fig. 3. (**A** to **D**) Schematic view of the structures of water clusters from the dimer (A) to pentamer (D) from experiment (A and B) or calculation (C and D), indicating the number and types of O–H bonds in each cluster. (**E**) Schematic view of a water molecule in which both hydrogens are donated to hydrogen bonds. (**F**) Schematic view of an O–H bond that is hydrogen-bonded to the π cloud of benzene. The orientation of the water cluster relative to benzene and the precise positions of the atoms in the cluster are not determined in the present work.

the gas-phase and matrix-isolated water dimer (Table 2). This result is consistent with the earlier rotational band contour analysis (*25*) of BW$_2$ in R2PI, which showed that the two water molecules are on the same side of the benzene ring (above the plane) at a center-of-mass separation close to that in the water dimer (Fig. 3A). On that basis, the band at 3550 cm^{-1} is assigned as the water-water hydrogen-bonded donor OH. An assignment of the other three transitions based on direct analogy with water dimer places the acceptor asymmetric stretch at 3722 cm^{-1}, the donor free O–H at 3708 cm^{-1}, and the acceptor symmetric stretch at 3608 cm^{-1}. This assignment (included in Table 2) views the acceptor water O–H stretch vibrations as delocalized over both O–H bonds despite the presence of benzene. Alternatively, if the benzene molecule orients one of the acceptor water O–H bonds toward the π cloud, then the 3608 cm^{-1} transition would be assigned as the π hydrogen-bonded O–H and the 3722 and 3708 cm^{-1} transitions would be donor and acceptor free O–H transitions, respectively. Rotationally resolved studies will be needed to distinguish these possibilities.

Pugliano and Saykally (*6*) have determined that the water trimer is a cyclic hydrogen-bonded structure in which all three water molecules donate one O–H to the H-bonded ring (Fig. 3B) with the other three hydrogens essentially free. The water trimer is also the largest water cluster for which O–H stretch data are available (*9, 11, 12*). The calculations of Xantheas and Dunning (*14*) on W$_3$ predict that the six O–H stretch vibrations are composed of one set of three near-degenerate transitions due to free O–H groups, and three hydrogen-bonded donor O–H vibrations shifted to much lower frequencies (−231, −240, and −299 cm^{-1}).

In the RIDIR spectrum for BW$_3$ (Fig. 2C), five of the six possible O–H stretch transitions are observed. The furthest blue transition is at 3716 cm^{-1}, consistent with an assignment as a free O–H stretch. The three highly red-shifted transitions (3550, 3508, and 3423 cm^{-1}), can be ascribed to singly hydrogen-bonded donor O–H groups in the cyclic water trimer. The peak at 3657 cm^{-1} does not match up with any transition in the pure water trimer. Both the small frequency shift from "free O–H" and the presence of similar bands in the BW$_4$ to BW$_7$ spectra argue for this transition's assignment as the O–H stretch of the O–H bond that is "hydrogen-bonded" (*28, 29*) to benzene's π cloud (Fig. 3F). The sixth O–H stretch (likely a free O–H stretch) is either unresolved or has negligible intensity. Thus, the transition frequencies in BW$_3$ can be accounted for as those of a cyclic W$_3$ cluster perturbed by benzene's presence. The major effects of benzene are to break degeneracies in the W$_3$ O–H stretch transitions and to induce some intensity in otherwise forbidden (*14, 15*) transitions.

A similar assignment scheme can be transferred to BW$_4$ and BW$_5$, both of which are predicted by calculations (*28, 34*) to incorporate cyclic W$_4$ and W$_5$ aggregates π hydrogen-bonded to benzene (Fig. 3, C and D). In keeping with this scheme, the spectra of Fig. 2, D and E, exhibit free O–H stretch transitions grouped around 3715 cm^{-1}, a single, narrow π hydrogen-bonded O–H stretch (~3650 cm^{-1}), and a group of single donor O–H stretch transitions centered on 3450 cm^{-1} in BW$_4$ and 3350 cm^{-1} in BW$_5$. In these larger clusters, Fermi resonance mixing of single donor stretches with overtones of the O–H bend may contribute to the low-frequency region of the spectrum. By BW$_5$ (Fig. 2E), the gap between the free O–H and the lowest frequency transitions has widened to more than 500 cm^{-1}.

The red-shifted single donor transitions in BW$_4$ and BW$_5$ provide the first clear evidence of broadening beyond the instrument-limited widths of smaller cluster transitions. The mode specificity of this broadening is evident in BW$_4$, whose free and π hydrogen-bonded O–H transitions (3724, 3713, and 3652 cm^{-1}) have widths of 3.5, 5, and 4 cm^{-1}, respectively, whereas the single donor O–H stretches are broadened to 7 (3461 cm^{-1}), 18 (3427 cm^{-1}), and 10 cm^{-1} (3367 cm^{-1}). This mode-selective broadening must arise from strong coupling of the O–H bonds in the hydrogen-bonded cycle (Fig. 3C) to intermolecular vibrations mediated by the network of hydrogen bonds. The widths of these transitions provide some measure of the homogeneous broadening inherent to networks of hydrogen bonds, a result of relevance to the breadths of the O–H absorptions in liquid water (*2*).

The spectrum of BW$_6$ is particularly intriguing because W$_6$ is the smallest water

Table 1. Frequencies and FWHM breadths (in parentheses) of the O–H stretch transitions (cm^{-1}) in C_6H_6-$(H_2O)_n$. Only the breadths of transitions that are not obviously overlapping have been included. The reported widths probably have some contribution from power broadening. Approximate errors are ±0.5 cm^{-1} in the upper left corner of the table and ±3 cm^{-1} in the lower right corner.

n = 1	n = 2	n = 3	n = 4	n = 5	n = 6	n = 7	Assignment
3785 (2.5)							Free O–H*
3774 (3.5)							
3748 (3.5)							
3740 (2.0)	3722 (≤7)	3716 (≤4)	3724 (3.5)	3719 (≤5)	3714	3713 (~13)	
3733 (2.0)	3708 (≤6)		3713 (5.0)	3714	3708		
3713 (2.5)							
		3657	3652 (4.0)	3646 (5)	3636 (9)	3636 (14)	π Hydrogen bond*
3634 (4)	3608 (3)						
					3578 (14)	3591	Double donor (n = 6, 7)†
						3580	
						3570	
	3550 (4.5)	3550 (6.5)			3508 (7.7)	3522 (8)	
		3508 (5)				3509 (8)	
					3453 (15)		
		3423 (4.5)	3461 (7)	3445	3408 (17)	3456 (12)	Single donor‡
			3427 (18)	3411			
			3367 (10)	3365?	3389 (20)	3294	
				3322 (~6)	3308 (17)	3280	
				3223 (11)	3210 (32)	3205 (12)	
				3185 (14)		3169 (20)	
					3078 (24)	3117 (13)	

*For $n \geq 3$. †For $n \geq 6$. ‡Approximate assignment for those transitions below the line in the table. Larger clusters may have contributions from O–H bend overtones in this region.

cluster for which noncyclic structures are predicted by calculation to be similar in energy to the cyclic hexamer (*14–21*). Table 2 lists O–H stretch vibrational frequencies calculated for the cyclic hexamer and a low-energy noncyclic (prismoidal) water hexamer. The differences in O–H stretch vibrational frequencies between cyclic and prismoidal W_6 structures is striking. The noncyclic water hexamer contains water molecules that donate both hydrogens to hydrogen bonds (Fig. 3E). These "double donor" stretches have frequency shifts in the -70 to -300 cm^{-1} region where the cyclic W_6 structure has no activity. Knochenmuss and Leutwyler (*16*) have concluded that these vibrations serve as a signature for the formation of more compact, noncyclic water structures.

Predictions for the W_6 clusters provide a remarkably useful guide to interpretation of the BW_6 spectrum. The spectrum of Fig. 2F shows 11 resolved transitions spread over the range from 3714 to 3078 cm^{-1}. The free O–H stretch transitions are centered on 3710 cm^{-1}, whereas the π hydrogen-bonded O–H stretch is slightly shifted to 3639 cm^{-1}. The single donor O–H stretch transitions extend from about 3400 cm^{-1} down into the C–H stretch region at 3078 cm^{-1}. Most importantly, even though in BW_5 there are no absorptions between 3445 and 3646 cm^{-1} (Fig. 2E), in BW_6 two transitions appear at 3508 and 3578 cm^{-1} (Fig. 2F). These transitions, and possibly those at 3453 and 3408 cm^{-1}, are assigned as double donor O–H stretches, providing experimental evidence that in BW_n clusters the changeover from cyclic to noncyclic W_n

Table 2. Comparison of the observed BW_n O–H stretch transitions with experimental and calculated W_n data. The frequency shifts are relative to the frequency of uncoupled OH in isolated H_2O, taken as the average of the symmetric and antisymmetric stretches; sym., symmetric; asym., asymetric.

n	Observed BW_n	Observed W_n	Observed BW_n frequency shift (cm^{-1})	Calculated W_n frequency† shift		Tentative BW_n assignment
1	3785		+79			Internal rotation of water built on ν_1, ν_3
	3774, 3748		+68, +42			
	3739, 3733	3756 (asym. stretch)	+33, +30			
	3713		+7			
	3634	3657 (sym. stretch)	−72			
2	3722	3745*	+16	+57‡		Acceptor asym. stretch
	3708	3730	+2	+35		Donor free O–H
	3608	3600	−98	−73		Acceptor sym. stretch
	3550	3530	−156	−160		Donor bridge O–H
3	3716	3707§	+10	+26, +24 +20		Free O–H
	3657		−49			π Hydrogen-bonded O–H
	3550	3516§	−156	−231		Single donor O–H
	3508	3400?, 3357?‖	−198	−240		
	3423	3340?, 3366?¶	−283	−299		
4	3724		+18	+15 (3)		Free O–H
	3713		+7	+14		
	3652		−54			π Hydrogen-bonded O–H
	3461		−245	−350		Single donor O–H
	3427		−279	−388 (2)		
	3367		−339	−481		
5	3719		+13	+14, +10		Free O–H
	3714		+9	+8, +7 +4		
	3646		−60			π Hydrogen-bonded O–H
	3445, 3411		−261, −295	−400, −410		Single donor O–H
	3365?, 3322		−341?, −384	−456, −466		
	3223, 3185		−479, −521	−549		
6	3714		+8	+9#	+16, +6**	Free O–H
	3708		+2	+8 (5)	+3, −1	+2
	3639		−67			π Hydrogen-bonded O–H
	3578		−128		−113	Double donor O–H
	3508		−198		−154	
	3453, 3408		−253, −298	−402	−208, −294	
	3389, 3308		−317, −398	−421 (2)	−352, −397	Single donor O–H
	3210, 3078		−496, −628	−479 (2) −554	−450, −670	

*Gas-phase results from (*8*). †For $n = 6$, the values for the cyclic and prismoidal structures are given to the left and right, respectively, of the line. ‡Calculated frequency shifts from an MP2/aug-cc-*p*VDZ ab initio calculation (*14*) for $n = 1$ through 4, and from a 6-31 + G(2*d,p*) calculation (*39*) for $n = 5$, 6. In the calculations of (*39*), the *d* functions are taken from aug-cc-*p*VDZ while the hydrogen *p* is from cc-*p*VDZ. Similar results for $n = 2$ through 5 were obtained in the scaled 4-31G calculations of (*15*, *16*). §Matrix data from (*12*). ‖Tentative assignment from gas-phase spectra of (*9*). ¶Tentative assignment from gas-phase spectra of (*11*). #6-31 + G(2*d,p*) vibrational frequencies for the cyclic water hexamer. **6-31 + G(2*d,p*) vibrational frequencies of (*39*) for the P1 prismoidal water hexamer structure calculated (*17*) to be among the lowest energy noncyclic W_6 structures.

cluster structures occurs at $n = 6$.

The IR spectrum of the dominant R2PI transition assigned to BW_7 (Fig. 2G) further confirms this interpretation. By comparison to the BW_6 spectrum, the spectrum of BW_7 transfers additional intensity from the free O–H stretch transitions at 3713 cm^{-1} to new bands in the region from 3500 to 3600 cm^{-1} ascribable to double donor O–H stretches. Thus, already by BW_7, the majority of water molecules donate both hydrogens to hydrogen bonds.

We cannot presently distinguish which of the several low-energy noncyclic W_n structures is present in BW_6 and BW_7. In fact, the R2PI spectra of Fig. 1, E and F, show weak features that may be attributable to other structural isomers; IR spectra of these features as well as IR spectra of even larger BW_n clusters are needed. Given the large number of calculated structures with nearly the same energy [Tsai and Jordan (*17*) found 20 W_6 structures within 2 kcal/mol of the lowest energy structure], the presence of benzene may alter the energy ordering of the W_n structures. Ultimately, calculations of the IR frequencies and intensities of the BW_n clusters themselves are needed for direct comparison with experiment.

REFERENCES AND NOTES

1. G. C. Pimentel and A. L. McClellan, *The Hydrogen Bond* (Freeman, San Francisco, 1960).
2. For a recent overview of the subject, see J. C. Pore and J. Texeira, Eds., *Hydrogen-Bonded Liquids* (Kluwer, Dordrecht, Netherlands, 1991).
3. Some examples of studies of liquid water and ice: T. C. Sivakumar, S. A. Rice, M. G. Sceats, *J. Chem. Phys.* **69**, 3468 (1978); M. S. Bergren, D. Schuh, M. G. Sceats, S. A. Rice, *ibid.*, p. 3477; J. P. Devlin, in *Proton Transfer in Hydrogen-Bonded Systems*, T. Bountis, Ed. (Plenum, New York, 1992).
4. T. R. Dyke and J. S. Muenter, *J. Chem. Phys.* **60**, 2929 (1974); J. A. Odutola and T. R. Dyke, *ibid.* **72**, 5062 (1980).
5. K. L. Busarow *et al.*, *ibid.* **90**, 3937 (1989); N. Pugliano and R. J. Saykally, *ibid.* **96**, 1832 (1992).
6. N. Pugliano and R. J. Saykally, *Science* **257**, 1937 (1992).
7. E. Zwart, J. J. ter Meulen, W. L. Meerts, L. H. Coudert, *J. Mol. Spectrosc.* **147**, 27 (1991).
8. Z. S. Huang and R. E. Miller, *J. Chem. Phys.* **91**, 6613 (1989).
9. D. F. Coker *et al.*, *ibid.* **82**, 3554 (1985).
10. M. F. Vernon *et al.*, *ibid.* **77**, 47 (1982); R. H. Page, J. G. Frey *et al.*, *Chem. Phys. Lett.* **106**, 373 (1984); R. H. Page *et al.*, *ibid.* **141**, 1 (1987).
11. S. Wuelfert, D. Herren, S. Leutwyler, *J. Chem. Phys.* **86**, 3751 (1987).
12. A. Engdahl and B. Nelander, *ibid.*, p. 4831.
13. R. M. Brentwood, A. J. Barnes, W. J. Orville-Thomas, *J. Mol. Spectrosc.* **84**, 391 (1980).
14. S. S. Xantheas and T. H. Dunning Jr., *J. Chem. Phys.* **99**, 8774 (1993).
15. E. Honegger and S. Leutwyler, *ibid.* **88**, 2582 (1988).
16. R. Knochenmuss and S. Leutwyler, *ibid.* **96**, 5233 (1992).
17. C. J. Tsai and K. D. Jordan, *Chem. Phys. Lett.* **213**, 181 (1993).
18. A. Vegiri and S. C. Farantos, *J. Chem. Phys.* **98**, 4059 (1993).
19. K. S. Kim *et al.*, *Chem. Phys. Lett.* **131**, 451 (1986); B. J. Mhin *et al.*, *J. Chem. Phys.* **100**, 4484 (1994).
20. K. F. Franken, M. Jalaie, C. E. Dykstra, *Chem. Phys. Lett.* **198**, 59 (1992); C. E. Dykstra, *J. Chem. Phys.* **91**, 6472 (1989).
21. K. Laasonen, M. Parrinello, R. Car, C. Lee, D. Vanderbilt, *Chem. Phys. Lett.* **207**, 208 (1993).
22. D. Belford and E. S. Campbell, *J. Chem. Phys.* **86**, 7013 (1987).
23. J. G. C. M. van Duijneveldt–van de Rijdt and F. B. van Duijneveldt, *J. Comput. Chem.* **13**, 399 (1992).
24. K. Szalewicz, S. J. Cole, W. Kolos, R. J. Bartlett, *J. Chem. Phys.* **89**, 3662 (1988).
25. J. R. Reimers, R. O. Watts, M. L. Klein, *Chem. Phys.* **64**, 95 (1982).
26. S. Zlanina, *Z. Phys. Chem.* **171**, 131 (1991).
27. A. Engdahl and B. Nelander, *J. Phys. Chem.* **89**, 2860 (1985).
28. A. J. Gotch and T. S. Zwier, *J. Chem. Phys.* **96**, 3388 (1992); A. W. Garrett and T. S. Zwier, *ibid.*, p. 3402. See also a review chapter by A. W. Garrett and T. S. Zwier to appear in *Advances in Multiphoton Processes and Spectroscopy*, vol. 9, S. H. Lin, A. A. Villaeys, Y. Fujimara, Eds. (World Scientific, River Edge, NJ, in press).
29. S. Suzuki *et al.*, *Science* **257**, 942 (1992).
30. H. S. Gutowsky, T. Emilsson, E. Arunan, *J. Chem. Phys.* **99**, 4883 (1993).
31. J. Wanna *et al.*, *ibid.* **85**, 1795 (1986).
32. P. Linse, *J. Comput. Chem.* **9**, 505 (1988).
33. J. D. Augspurger, C. E. Dykstra, T. S. Zwier, *J. Phys. Chem.* **96**, 7257 (1992).
34. ______, *ibid.* **97**, 980 (1993).
35. R. H. Page, Y. R. Shen, Y. T. Lee, *J. Chem. Phys.* **88**, 4621 (1988).
36. BW_n clusters are formed in a pulsed supersonic expansion into which metered flows of benzene (0.1%) and water (0.2 to 0.4%) are mixed in helium at a total backing pressure of 4 bar.
37. A grating-tuned $LiNbO_3$ OPO pumped by the far-field, unseeded 1.06-μm output of a Nd:yttrium-aluminum-garnet laser (Continuum NY61-20) produces ~5 mJ per pulse over the region from 2800 to 4000 cm^{-1} of interest here. The bandwidth of the OPO is about 1 cm^{-1}.
38. R. N. Pribble and T. S. Zwier, unpublished results.
39. K. Kim and K. D. Jordan, unpublished results.

40. This work was supported by the National Science Foundation and by an equipment grant to build the OPO from Continuum, Inc. We thank K. Haber and A. Garrett for their part in the early setup of the OPO. We also thank J. Lisy for lending us a $LiNbO_3$ crystal during the early characterization of our OPO.

14 January 1994; accepted 6 April 1994

Deep Seismic Expression of an Ancient Plate Boundary in Europe

Alet Zielhuis and Guust Nolet

Seismological results on the structure of the upper mantle below Europe reveal a marked contrast in seismic properties between Precambrian and younger parts of Europe. The Precambrian craton in eastern Europe is characterized by high shear-wave velocities, which can be explained by low temperatures. The transition to low seismic velocities below Phanerozoic Europe coincides with the crustal boundary zone of the craton and exists to depths of at least 140 kilometers. Despite the long and complex tectonic history of the plate boundary zone, the transition is remarkably sharp, which rules out any significant lateral transport of asthenospheric material across the suture zone.

Western and eastern Europe have distinctly different geological histories. Precambrian eastern Europe has been stable since Late Precambrian times. In contrast, western Europe was formed during Phanerozoic accretion to the Precambrian continent. At crustal levels the boundary between the two tectonic provinces is formed by an ancient suture zone, the Tornquist-Teisseyre zone (TTZ). Stretching from south Sweden to the Black Sea, the TTZ is Europe's largest tectonic lineament. Previous seismological studies (*1*) have shown that eastern and western Europe have different upper mantle structures, but little has been known about the character, exact location, and depth of the transition between the structures. To investigate this ancient plate boundary, we discuss a detailed three-dimensional model for the shear-wave velocity in the upper mantle below Europe (*2*). This model was obtained by waveform inversion of both body and surface waves, recorded on vertical-component seismograms (*3*). Using relatively short paths and high frequencies (up to 60 MHz) we obtained a lateral resolution of about 200 km locally, which compares very favorably with the resolving power of 1000 to 2000 km in current global models of shear-wave velocity variations (*4–11*). The incorporation of higher modes of Rayleigh waves gives a depth resolution of 90 km at a depth of 80 km and 150 km at a depth of 400 km, which is superior to that of most fundamental mode studies. The three-dimensional model reveals that the TTZ is not only discernible at crustal depths but that it also forms an important boundary at upper mantle levels.

The Precambrian craton, consisting of the Baltic shield and Russian platform, is characterized by high shear-wave velocities (Fig. 1, A and B). The sharp transition to lower velocities of the Phanerozoic regions of western Europe coincides with the TTZ. Laterally, the velocity contrast

---

A. Zielhuis, Research School of Earth Sciences, The Australian National University, Canberra ACT 0200, Australia.
G. Nolet, Department of Geological and Geophysical Sciences, Guyot Hall, Princeton University, Princeton, NJ 08544, USA.